ACS OMEGA

Open Access

http://pubs.acs.org/journal/acsodf

Article

Tracking Selective Internalization and Intracellular Dynamics of Modified Chitosan Polymeric Micelles of Interest in Primary Hyperoxaluria Diseases

María Ángeles Fernández-Mimbrera, Sofía Salido, Juan Alberto Marchal, and Alfonso Alejo-Armijo*

Cite This: *ACS Omega* 2024, 9, 39503−39512

Read Online

ACCESS | Metrics & More | Article Recommendations | Supporting Information

ABSTRACT: Primary hyperoxalurias (PHs) represent rare diseases associated with disruptions in glyoxylate metabolism within hepatocytes. Impaired glyoxylate detoxification in PH patients results in its accumulation and subsequent conversion into oxalate, a process catalyzed by the hepatic lactate dehydrogenase A enzyme (*h*LDHA). Targeting this enzyme selectively in the liver using small organic molecules emerges as a potential therapeutic strategy for PH. However, achieving selective hepatic inhibition of *h*LDHA poses challenges, requiring precise delivery of potential inhibitors into hepatocytes to mitigate adverse effects in other tissues. Our recent efforts focused on the design of polymeric micelle nanocarriers tailored for the selective transport and release of *h*LDHA inhibitors into liver tissues. In this study, we synthesized and assessed the internalization and disaggregation dynamics of chitosan-based polymeric micelles in both hepatic and nonhepatic cell models using live-cell imaging. Our findings indicate that lactonolactone residues confer internalization capacity to the micelles upon exposure to cells. Moreover, we demonstrated the intracellular disaggregation capacity of these nanocarriers facilitated by the cystamine redox-sensitive linker attached to the polymer. Importantly, no cytotoxic effects were observed throughout the experimental time frame. Finally, our results underscore the higher selectivity of these nanocarriers for hepatic HepG2 cells compared to other nonhepatic cell models.

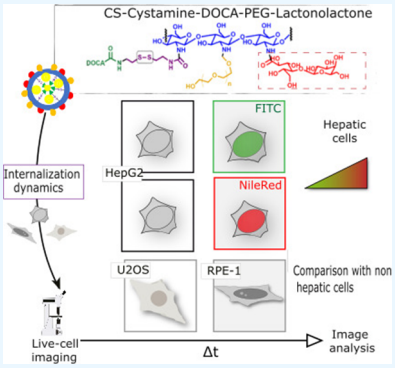

1. INTRODUCTION

Primary hyperoxalurias (PHs) constitute a group of rare diseases characterized by a hepatic genetic disorder related to glyoxylate metabolism, leading to abnormal overproduction of oxalate.[1−3] This terminal metabolite is synthesized in the liver and excreted by the kidneys, where the excess of oxalate can precipitate as calcium oxalate crystals or stones, ultimately resulting in kidney failure, often progressing to end-stage renal disease.[4,5] Glyoxylate detoxification involves three key enzymes: (i) alanine-glyoxylate aminotransferase, (ii) glyoxylate reductase-hydroxypyruvate reductase, and (iii) 4-hydroxy-2-oxoglutarate aldolase.[6] Malfunctions or defects in these enzymes lead to an imbalance in the glyoxylate concentration. Under such conditions, alternative pathways are activated to reduce its concentration, involving the action of lactate dehydrogenase A (LDHA), which rapidly catalyzes the oxidation of glyoxylate to oxalate as the terminal metabolite (Figure 1).

Among the various enzymes involved in liver glyoxylate metabolism, LDHA and glycolate oxidase (GO) have been identified as potential and safe targets for PH treatment.[5,7] Two different approaches have been pursued to selectively achieve their inhibition: (i) *si*RNA inhibition of GO[8,9] or LDHA[10−12] and (ii) inhibition of the active sites in GO,[13,14] LDHA,[15−17] or both[18,19] using small molecules. The advantage of targeting LDHA lies in its role in the final stage of glyoxylate metabolism, directly catalyzing oxalate formation, thereby reducing cytosolic levels of this terminal metabolite and offering a comprehensive treatment for all PH types.

Recognizing the necessity for selective LDHA isoenzyme inhibition, mainly found in liver and muscle tissues,[20,21] our research group has focused on designing and synthesizing selective LDHA isoenzyme inhibitors in the past few years.[15−17] However, selectively targeting LDHA in hepatocytes poses a challenge to its use as a treatment for PHs, and specific transporters for these inhibitors need to be developed.

Polymeric micelles, particularly those with a chitosan core, have gained significant interest as drug delivery systems for treating various diseases.[22−24] This interest stems from their inherent biocompatibility and biodegradability, as well as their chemical versatility, unique structure, size, and morphology.[25] The encapsulation of hydrophobic drugs within these polymeric systems offers several advantages over free drug

Received: April 9, 2024
Revised: July 24, 2024
Accepted: August 20, 2024
Published: September 10, 2024

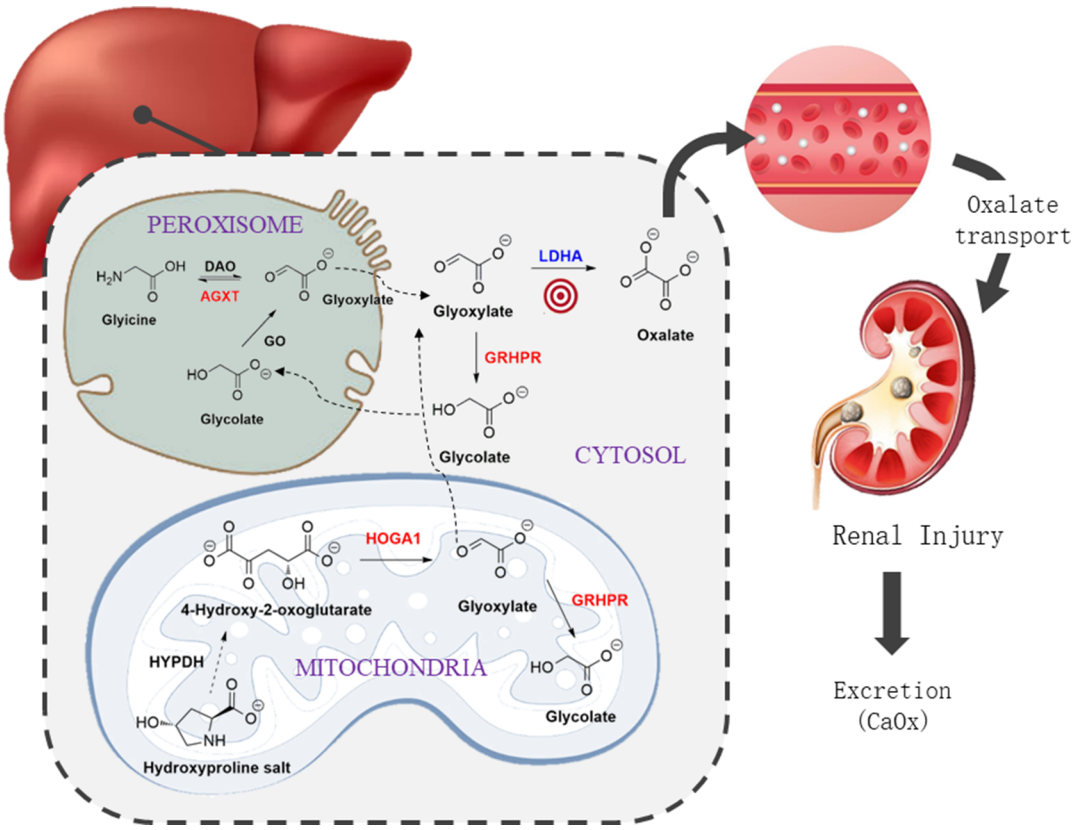

Figure 1. Metabolic pathways of glyoxylate detoxification. Enzymes involved in PHs are highlighted in red.

forms, including improved stability, solubility, and bioavailability.[25,26] Additionally, owing to their chemical flexibility, polymeric micelles can be easily modified with specific ligands, enhancing their specificity and targetability toward selected tissues or cell lines. The aforementioned modifications facilitate increased drug accumulation in the targeted tissue while minimizing the risk of nonspecific tissue toxicity.[26] These properties position polymeric micelles as promising candidates for the treatment of pathologies requiring tissue specificity and recognition, such as PHs.

With this idea in mind, our research group has been developing a redox-sensitive nanocarrier system based on polymeric micelles with a chitosan core for the targeted delivery of LDHA inhibitors into hepatocytes.[27] These polymeric micelles incorporate a redox-sensitive moiety (cystamine linker), responsive to the high intracellular glutathione (GSH) concentration in hepatocytes.[28] Additionally, they include a directing ligand (lactonolactone) recognized by asialoglycoprotein receptors (ASGPRs), which are overexpressed in hepatocyte cell membranes.[29] In that sense, the chitosan polymer was specifically grafted for both the selective recognition of hepatocytes against other cell types and their disassembly inside them to release their cargo.

While the stability and disaggregation abilities of these polymeric micelles concerning GSH concentration have been simulated in silico by us,[27] a more detailed analysis of their selective internalization and dynamic disaggregation within hepatocytes and other cell types is necessary for further development and optimization of the material previously prepared and characterized by us. In this study, we synthesized and assessed the internalization and disaggregation capacities of different chitosan-based polymeric micelles using hepatic and nonhepatic cellular models. To evaluate their capacity as nanocarriers for the treatment of PHs, we selected two fluorescent probes, fluorescein isothiocyanate (FITC) and Nile Red, for being encapsulated during micelle synthesis. Both fluorophores are commonly used for staining and tracking the intracellular dynamics of similar nanocarriers.[30−33] The combination of both fluorophores allows us to not only evaluate internalization but also predict the disassembly capacity of micelles under natural living conditions. For this purpose, we employed confocal live-cell microscopy, a methodology providing more reliable and comprehensive information compared with fixed-cell-based approaches, enabling dynamic visualization of the fluorophore signal in live cells over time. Moreover, the physiological status and viability of cells were monitored concurrently, which is crucial for the biological applicability of these polymeric micelles.

2. EXPERIMENTAL SECTION

2.1. Materials. Solvents and starting materials used were obtained from commercial sources and were used without further purification. Specifically, Nile Red was purchased from TCI Europe (Zwijndrecht, Belgium) and FITC from Abcam (Cambridge, United Kingdom). Dulbecco's modified Eagle's medium (DMEM) supplemented with 10% fetal bovine serum (FBS) and antibiotics (1% Penicillin-Streptomycin) was purchased from Gibco (ThermoFischer Scientific, Carlsbad, California, United States). Chitosan-based polymeric materials **1**−**4** were also prepared and characterized according to the methodology previously described by us.[27]

Cell lines used were purchased from American Type Culture Collection (ATCC, Manassas, Virginia, United States) or kindly provided. In particular, hepatocellular carcinoma cells

https://doi.org/10.1021/acsomega.4c03415
ACS Omega 2024, 9, 39503−39512

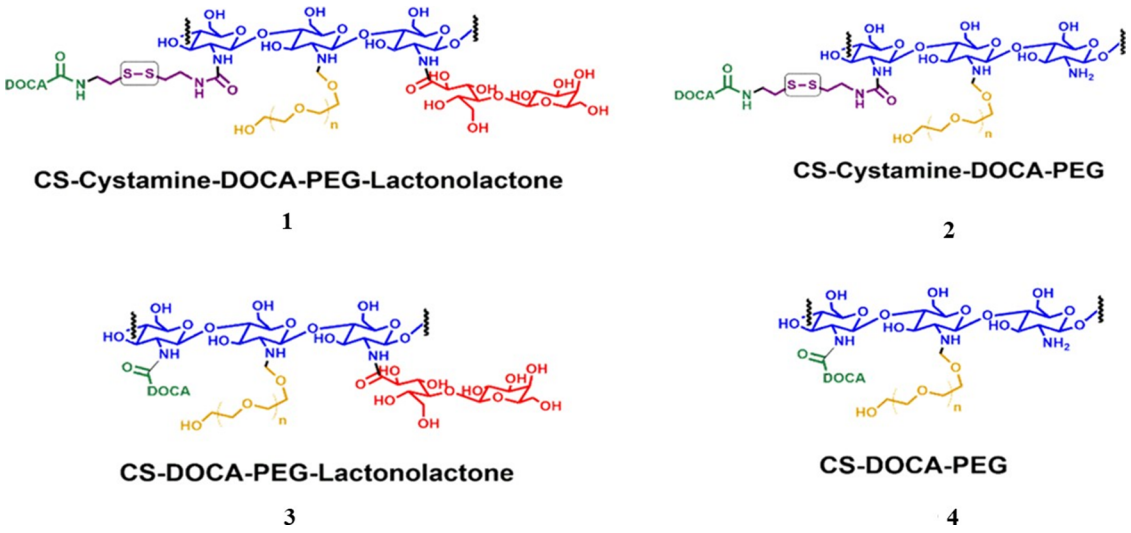

Figure 2. Structure of the polymeric micelles. Blue, chitosan core; green, DOCA moiety; purple, redox-sensitive cystamine linker; yellow, PEG moiety; red, lactonolactone.

(HepG2) were purchased from ATCC, retinal pigmented epithelial cells (*h*TERT RPE-1) were kindly provided by F. Cortés-Ledesma from *Centro Nacional de Investigaciones Oncológicas* (CNIO, *Instituto de Salud Carlos III*, Madrid, Spain),[34] and osteosarcoma cells (U2OS) were also kindly provided by H. Neitzel from Charite Hospital (Berlin, Germany).[35]

2.2. Drug-Loading and Entrapment Efficiency. All polymeric micelles (**1**−**4**) were formed following a two-step methodology involving dialysis and sonication, which we have previously used and optimized.[27] In that sense, polymers **1**−**4** (10 mg) were dissolved in 10 mL of H_2O with some drops of HOAc, then dialyzed for 3 days, and finally sonicated for 10 min using the probe-type ultrasonicator previously described. Then, 0.5 mL of a solution of FITC or Nile Red at 30 mg/mL in dimethyl sulfoxide was added dropwise to each polymeric micelle solution. The resulting suspension was energetically stirred at room temperature for 24 h and dialyzed against 1 L of deionized water for 24 h using a membrane with a molecular weight cutoff (MWCO) of 12 kDa. Finally, the micelle solution was filtered through a 0.5 μm filter and then lyophilized.

The entrapment efficiency (EE) and drug-loading efficiency (DL) were calculated using the following equations:

$$\mathrm{EE} = \frac{m_{\mathrm{f,micelles}}}{m_{\mathrm{f,total}}} \times 100\% \quad (1)$$

$$\mathrm{DL} = \frac{m_{\mathrm{f,micelles}}}{m_{\mathrm{f,total}} + m_{\mathrm{p,total}}} \times 100\% \quad (2)$$

where $m_{\mathrm{f,micelles}}$ is the mass (mg) of fluorescent compound in micelles, $m_{\mathrm{f,total}}$ is the total mass (mg) of fluorescent compound used, and $m_{\mathrm{p,total}}$ is the total mass (mg) of polymer (**1**−**4**) used.

The amount of nonencapsulated FITC or Nile Red in each polymeric micelle (**1**−**4**) was measured by UV−vis spectroscopy using a Genesys 150 Vis/UV−vis spectrophotometer (Thermo Fischer Scientific, Waltham, MA, USA) and calculated from standard curves obtained for FITC (y = 0.0013x + 0.0436; R^2 = 0.991) or Nile Red (y = 0.1673x + 0.0097; R^2 = 0.999) in EtOH:H_2O (1:1).

2.3. Polymeric Micelle Preparation for Cellular Analyses. Fluorescent-loaded micelles of polymers **1**−**4** were also prepared according to the methodology described in Section 2.2. Briefly, 5 mg of each polymer was dissolved in 5 mL of DMEM medium with a few drops of acetic acid (HOAc). Then, the mixture was dialyzed against 500 mL of DMEM medium (MWCO 12 kDa; Spectrum Laboratories Inc., USA) at room temperature for 3 days and sonicated for 10 min at 4 °C using a probe-type ultrasonicator (JY 92-2D; Ningbo Scientz Biotechnology Co., Ltd, Nanjing, China) at 100 W. Finally, all samples were filtered with a poly(ether sulfone) HPLC filter (0.22 μm).

2.4. Cell Culture Procedures. Cell culture was conducted under standard conditions, in a humidified atmosphere under 5% CO_2 at 37 °C using DMEM supplemented with 10% FBS and antibiotics (1% Penicillin-Streptomycin). Cells were split every 2 or 3 days depending on their proliferation rate. Viability and cell response were monitored through visual inspection under a microscope. The presence of mycoplasma was routinely checked using the MC-Venor GeM qEP mycoplasma detection kit (Minerva Biolabs) to ensure they were contamination-free.

2.5. Live-Cell Microscopy. For live imaging, 25,000−35,000 cells were plated onto eight-well slides ("μ-slide 8 well high Glass Botton #1.5H D263 Schott glass; Ibidi) and cultured under standard conditions. After 24 h, cells were washed three times and replaced with prewarmed DMEM without phenol red and without FBS. This medium also contained the corresponding micelles at the required concentration. As the control, parallel samples incubated with similar media but lacking micelles were always maintained. Cells were incubated with micelles for the next 3 h, and after that, washing-out and adding of a new medium were performed. Cells were immediately transferred to a microscope humidified stage incubator containing 5% CO_2 at 37 °C, coupled to an inverted laser scanning Leica TCS SP5 microscope. Cells were filmed with three to seven z sections with a 20× objective and 2× zoom using the Confocal LAS AF software (Leica Application Suite for Advanced Fluorescence). Images were acquired every 20 min, and live recording was extended during the next 6−12 h. For each data point,

https://doi.org/10.1021/acsomega.4c03415
ACS Omega 2024, 9, 39503−39512

transmitted light and either 488 (FITC fluorophore) or 561 (Nile Red fluorophore) laser scanning images were obtained. TIFF images were stacked and processed using FiJi.[36] For quantification data, maximum Z-projections were generated, and signal intensity data were obtained after manual selection of the ROI in FiJi. A minimum of 20 cells were inspected for each condition. Plots and statistical comparisons were done using RStudio (RStudio Team (2020). RStudio: Integrated Development for R. RStudio, PBC, Boston, MA URL http://www.RStudio.com/). Mean intensity data from a minimum of 20 cells were normalized against the mean value of the data from HepG2 cells. Statistical comparisons for the mean and median data were performed by Student's t and Wilcoxon's (W) tests, respectively. ****$p < 0.001$

3. RESULTS AND DISCUSSION

3.1. Polymeric Micelle Preparation and Encapsulation of Fluorescent Probes. Chitosan-based polymeric micelles **1**−**4** (Figure 2) were recently prepared, characterized, and described by our research group[27] as a smart nanocarrier-based drug delivery system targeting the hepatic lactate dehydrogenase A enzyme selectively inside hepatocytes. The chitosan core of all polymeric micelles was decorated with poly(ethylene glycol) (PEG, shown in yellow in Figure 2) and deoxycholic acid (DOCA, shown in green in Figure 2). Chitosan, known for its biocompatibility and nontoxic nature, was chosen as the core material.[25] DOCA was incorporated as the amphiphilic component to facilitate the self-aggregation of the polymers.[37] Furthermore, PEG was grafted onto the polymeric core to improve the stability and hydrophilicity of the resulting conjugates.[38] Additionally, polymeric micelles **1** and **3** were decorated with lactonolactone (shown in red in Figure 2), a ligand recognized by hepatocyte cells, and polymeric micelles **1** and **2** also included a redox-sensitive moiety (cystamine, shown in purple in Figure 2) to facilitate their disassembly and cargo release preferably inside hepatocytes where the concentration of GSH is high enough. The lactonolactone moiety has a terminal unit of galactose that allows recognition by ASGPRs highly expressed in hepatocytes.[29]

To study the internalization and disassembly processes of these polymeric micelles, two different fluorescent compounds were selected for encapsulation studies: (i) Nile Red, whose fluorescence is highly dependent on the environment and only fluoresces in hydrophobic media;[39] and (ii) FITC, which can emit fluorescence in both hydrophilic and hydrophobic environments and only fluoresces inside cells if properly internalized. Both fluorophores are nontoxic and widely used for cell staining.

Both complementary fluorophores were encapsulated inside polymeric micelles prepared (**1**−**4**) using a simple dialysis method previously used by us.[27] Table 1 shows the main encapsulation features of the fluorescent polymeric micelle systems.

In general terms, all polymeric micelles prepared showed high drug loadings (14.3−21.7%) and entrapment efficiencies (24.8−35.6%) for both selected fluorescent probes. According to the data obtained, it seems that Nile Red is slightly better encapsulated inside the polymeric micelle assayed.

3.2. Internalization and Disassembly of Polymeric Micelles into Hepatocytes. To investigate whether the lactonolactone moiety could properly recognize HepG2 cells and subsequently accumulate inside them, we employed confocal live-cell microscopy. This methodology allowed us to evaluate the signal distribution and intensity inside the same cell over time under physiological conditions. For this purpose, cells were incubated for 3 h with the corresponding FITC-encapsulated micelles (1 mg/mL), and live-cell recording was started immediately after the washout (experimental setup in Figure 3a). As shown in Figure 3b, remarkable fluorescence was observed inside HepG2 cells only when the lactonolactone moiety was attached to the chitosan core, i.e., polymeric micelles **1** and **3**. In parallel, cells treated under the same conditions but not exposed to micelles were also analyzed to exclude the occurrence of autofluorescence (Supplementary Video 3). Importantly, in all of our analyses, cells maintained a healthy condition similar to control cells (i.e., not exposed to micelles) during the experiments (Supplementary Videos 1−3). This indicates the lack of cytotoxic effects for the polymeric micelles evaluated under the indicated conditions.

HepG2 cells incubated with FITC-encapsulated micelles lacking the lactonolactone moiety (micelles **2** and **4**) did not show intracellular fluorescence (Figure 3b). Our data clearly demonstrate that lactonolactone residues are required for the internalization of micelles inside HepG2 cells. These results are in consonance with previous studies, suggesting a specific interaction of lactonolactone residues with the ASGPR ligand receptor located on the hepatocyte's surface.[32,40] Therefore, lactonolactone-mediated recognition at the cell surface allowed rapid internalization of the polymeric micelles, while passive diffusion practically did not occur.

Furthermore, our analyses allowed for a detailed investigation of the micelle dynamics inside the cells. The observed distribution of the FITC signal inside HepG2 cells was homogeneous and very similar for micelles **1** and **3**. As observed in Figure 3c, fluorescence accumulated not only throughout the cytoplasm but also inside the nuclei with the same intensity. This could indicate that polymeric micelles also have the capacity to cross the nuclear membrane and accumulate inside the nuclei or that free FITC released in the cytosol could diffuse to the nucleus (more details below). Moreover, this pattern of distribution was maintained during the time that the cells were monitored (Figure 3d). Our data also reveal a progressive reduction of the signal inside cells during the time course of the experiment, presumably due to the diffusion of fluorescent materials out of the cell, as previously observed by others.[33] During all this time, cells remained viable and had a normal appearance (Figure 3d).

Table 1. Encapsulation Features of the Fluorophore Loaded into Polymeric Micelles (1−4)[a]

polymeric micelle	fluorophore	entrapment efficiency (%) (EE)	drug loading (wt %) (DL)
1	FITC	26.5 ± 0.5	16.0 ± 0.2
	Nile Red	28.0 ± 0.4	17.2 ± 0.1
2	FITC	30.4 ± 0.6	16.5 ± 0.1
	Nile Red	ND[b]	ND[b]
3	FITC	24.8 ± 0.3	14.3 ± 0.1
	Nile Red	35.6 ± 0.3	21.7 ± 0.2
4	FITC	28.1 ± 0.4	16.5 ± 0.2
	Nile Red	ND[b]	ND[b]

[a]Data are represented as mean ± SD (n = 3). [b]ND, not determined. Polymeric micelles without lactonolactone are not able to internalize cells and therefore were not used for Nile Red release experiments (see Sections 3.2 and 3.3). For that sense, EE and DL were not measured for polymeric micelles **2** and **4** with Nile Red.

https://doi.org/10.1021/acsomega.4c03415
ACS Omega 2024, 9, 39503−39512

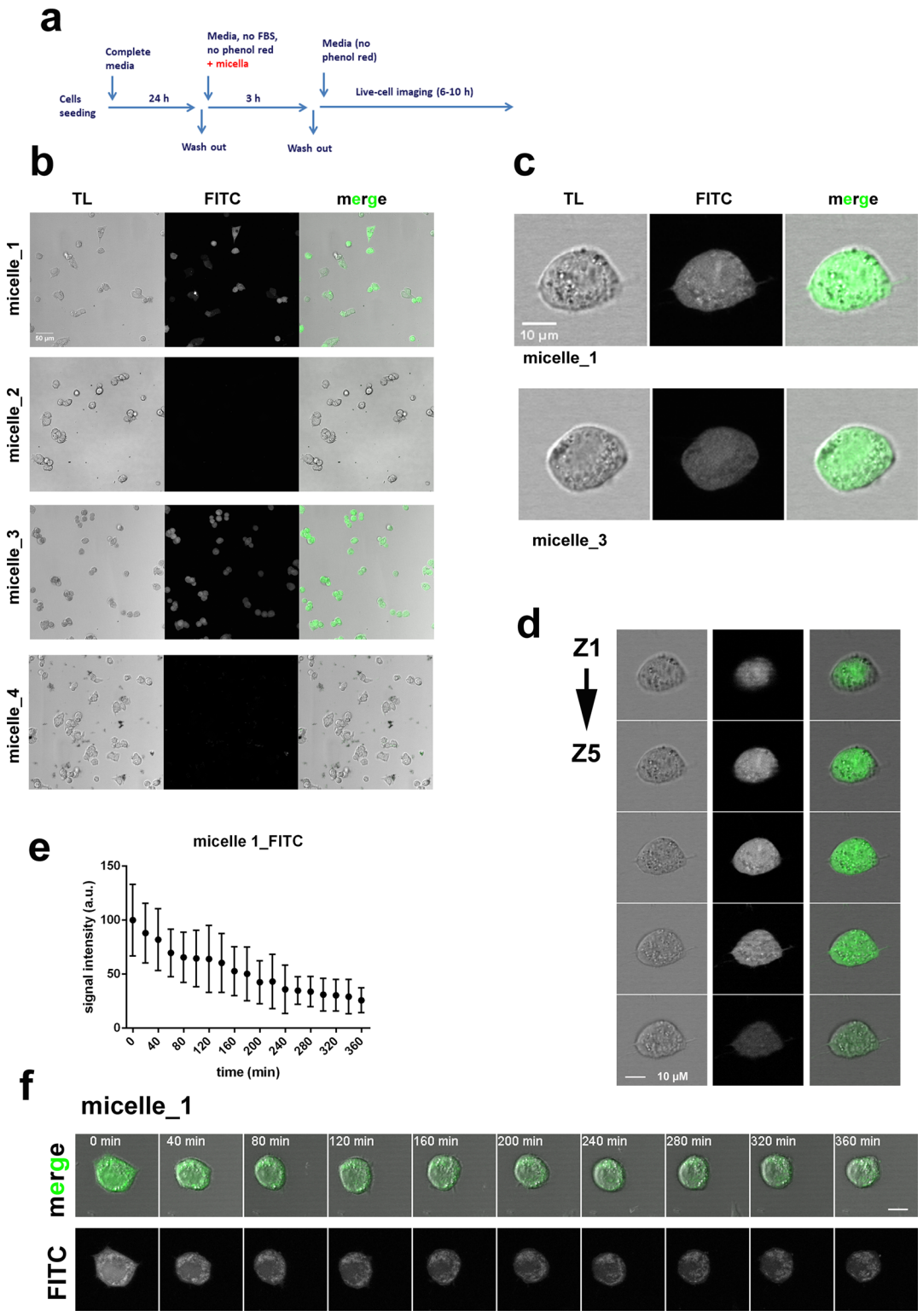

Figure 3. Internalization dynamics of FITC-encapsulated micelles in HepG2 cells. (a) Description of the experimental procedure employed. (b) Representative images obtained from confocal live-cell microscopy after 3 h of incubation with the corresponding micelles. All samples were processed in parallel under the same conditions. (c) Examples of cells magnified from (b), incubated with micelles **1** and **3**. Note that the FITC signal is homogeneously distributed through the cell. Maximum Z-projections are presented. (d) Z-stack images for one representative cell from upper C. (e) Relative quantification of the mean intensity FITC signal during the time course of the live-cell recording. For each time point, a minimum of 20 cells were selected and quantified. Data were normalized against the mean intensity value observed at time 0. Mean and SD values are presented. (f) Selected frames showing the FITC signal and cell dynamics upon time. Minutes from live-cell starting are shown. Scale bar is 5 μM..

The results obtained with FITC-encapsulated micelles **1** and **3** confirmed the internalization capacity of these nanocarriers based on their lactonolactone residues when exposed to HepG2 cells. However, the predicted disassembly capacity of

https://doi.org/10.1021/acsomega.4c03415
ACS Omega 2024, 9, 39503−39512

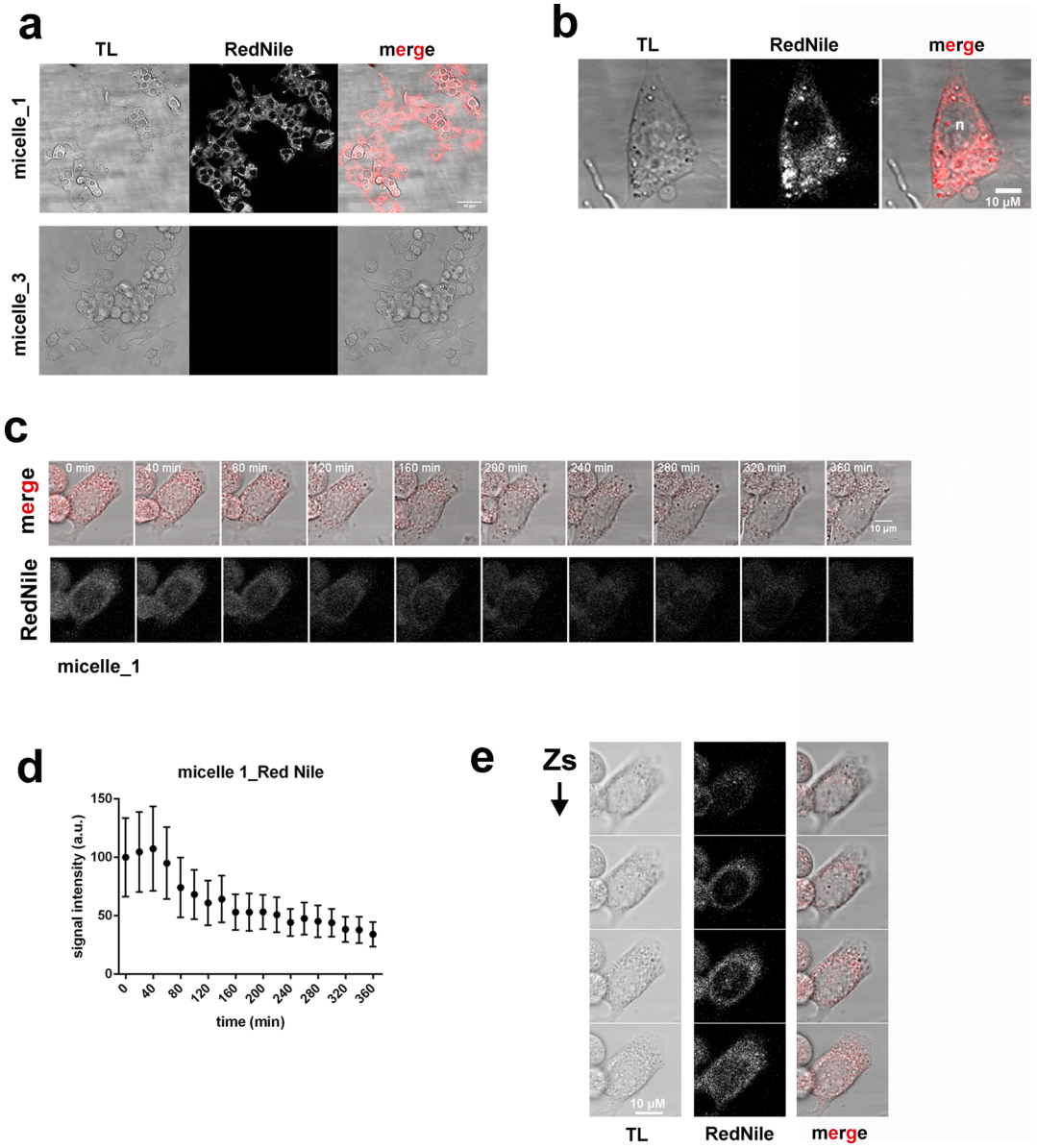

Figure 4. Internalization dynamics of Nile Red-encapsulated micelles in HepG2 cells. (a) Representative images obtained from confocal live-cell microscopy after 3 h of incubation with the corresponding micelles. All samples were processed in parallel under the same conditions. (b) Example of a cell magnified upon incubation with Nile Red-encapsulated micelle **1**. Note that the Nile Red signal is not included in the nuclei (n) in comparison with the FITC signal, which spreads through the nuclei (see Figure 3). Maximum Z-projections are presented. (c) Selected frames showing the Nile Red signal and cell dynamic upon time. Minutes from live-cell starting are shown. (d) Relative quantification of the mean intensity Nile Red signal during the time course of the live-cell recording. For each time point, a minimum of 20 cells were selected and the mean intensity value was quantified. Data were normalized against the mean intensity value observed at time 0. Mean and SD values are presented. (e) Z-stack images for the cell in (c) at time 0.

micelle **1** inside an intracellular media with a high concentration of GSH, typical in hepatocytes,[28] could not be established in our previous experiments. This is because the FITC dye exhibited a fluorescent signal both when encapsulated within the micelle and as a free form upon micelle disaggregation. To resolve this question, we made use of Nile Red, a dye that only fluoresces when interacting as a free form with the hydrophobic part of the cytosol.[41] The results obtained for polymeric micelles **1** and **3** encapsulated with Nile Red and exposed to HepG2 followed the same protocol explained before and are presented in Figure 4. While a clear fluorescent signal was detected inside cells for micelle **1**, no signal was observed for micelle **3** (Figure 4a). These results clearly demonstrate that micelle **1** is able to internalize HepG2 cells and disassemble inside them, as predicted, based on its cystamine-based redox-sensitive moiety. Moreover, these findings are in accordance with our previous observations in terms of disaggregation abilities of micelles **1** and **3**,[27] where we mimicked the reducing condition inside and outside hepatocytes using different GSH concentrations for micelles **1** and **3**, and we controlled the disassemble process by DLS, NMR-^{1}H, and HPLC-MS.[27]

We also investigated the dynamics of the Nile Red signal inside HepG2 cells. Compared with FITC-encapsulated micelles, a remarkable difference was the lack of signal inside the nuclei for the Nile Red micelles (see Figure 4b). A similar

https://doi.org/10.1021/acsomega.4c03415
ACS Omega 2024, 9, 39503−39512

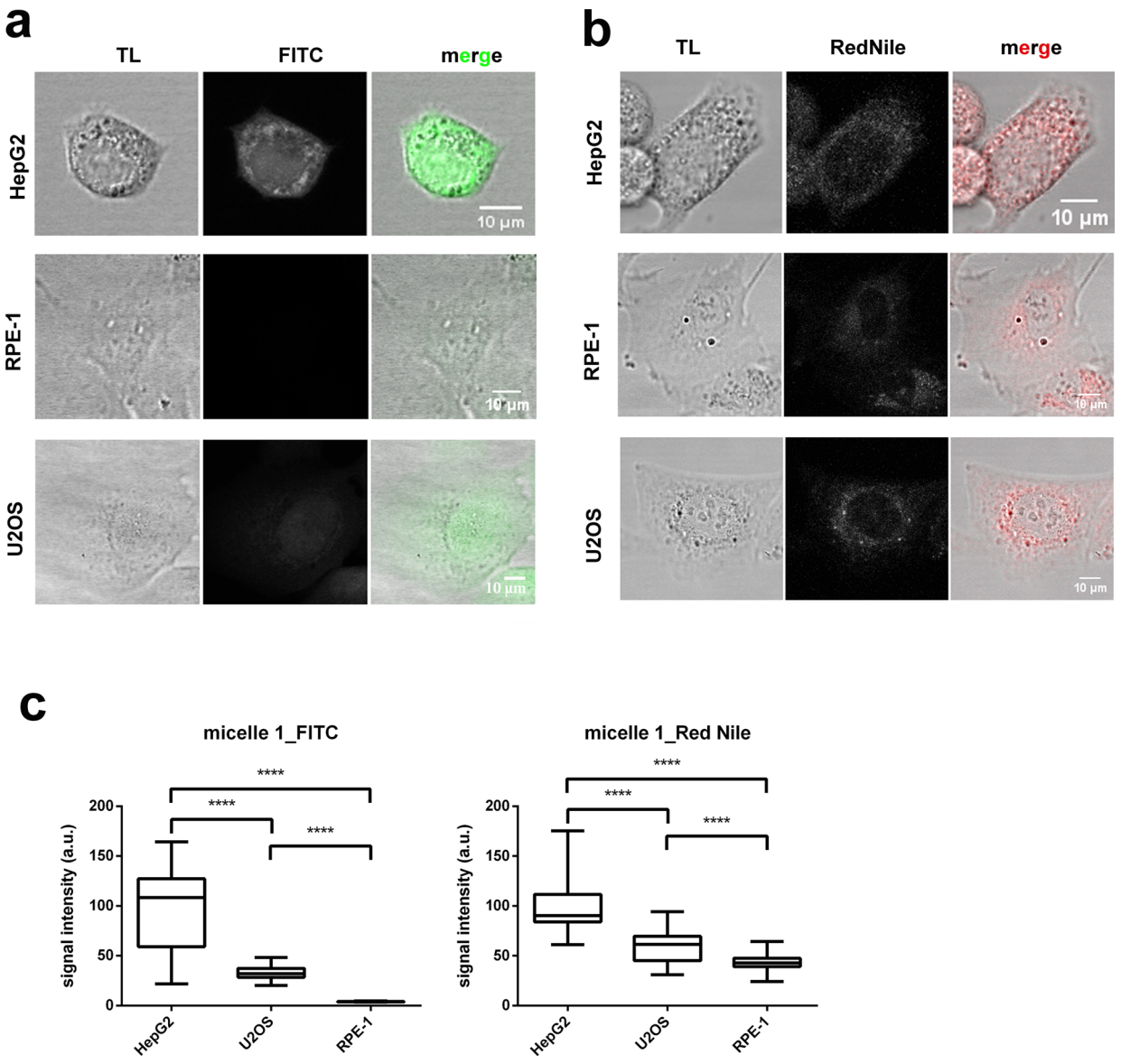

Figure 5. Internalization dynamics in other cell types. (a) Examples of HepG2 (upper panel), RPE-1 (middle panel), and U2OS (lower panel) cells after 3 h of incubation with FITC-encapsulated micelle **1**. (b) Examples of HepG2 (upper panel), RPE-1 (middle panel), and U2OS (lower panel) cells after 3 h of incubation with Nile Red-encapsulated micelle **1**. In both (a) and (b), images were obtained through confocal live-cell microscopy following the same experimental setup explained before. (c) Relative quantification of the mean intensity signal for FITC and Nile Red in the indicated cell lines. Mean intensity data from a minimum of 20 cells were obtained in each case and normalized against the mean value of the data from HepG2 cells. Statistical comparisons for the mean and median data were performed by Student's *t* and Wilcoxon's (W) tests respectively. ****$p < 0.001$.

pattern has been described before for other cell lines as A549 or BxPC3 when exposed to nanoparticles encapsulated with this fluorophore.[42,43] The hydrophilic composition of the nucleoplasm might inhibit the Nile Red fluorescence. The FITC signal, however, remains unaltered, either as a free form or encapsulated. Taking together both results, the FITC and Nile Red encapsulation, it is clear that micelle **1** has the ability to internalize and disassemble inside HepG2 cells (FITC and Nile Red fluorescence, Figures 3 and 4, respectively), while micelle **3** can internalize but not disassemble (only FITC fluorescence, Figure 3). Thus, the fluorescent signal observed in the nucleus for micelle **3** with FITC is mainly attributed to the presence of polymeric micelles with encapsulated FITC as micelle **3** does not release the encapsulated dye.

The distribution pattern described for Nile Red was maintained during the time that cells were monitored by live-cell microscopy, but the intensity of the signal progressively reduced over time (see Figure 4c), similar to what was previously observed for FITC.

3.3. Internalization and Disassembly of Polymeric Micelles into Other Cell Types. One of our key objectives was to determine the selectivity of polymeric micelles for the target cell type, i.e., hepatocytes. Our investigations were conducted using a hepatocellular carcinoma cell model, HepG2, which is widely employed in similar studies.[32,44] Consequently, we selected a nonhepatic cancer cell model to assess the internalization and cellular dynamic of micelle **1** encapsulated with either FITC or Nile Red. For this purpose, we chose osteosarcoma U2OS cells due to their flattened and

https://doi.org/10.1021/acsomega.4c03415
ACS Omega 2024, 9, 39503−39512

increased size, which are suitable for fluorescent microscopy analyses.[45] The results are presented in Figure 5. When compared with HepG2 cells treated under the same conditions, U2OS cells incubated with FITC-encapsulated micelle **1** exhibited a reduced signal, mainly accumulated in the nuclei (Figure 5a). Similar results were obtained when the analysis was repeated with Nile-Red-tagged micelle **1**. In this case, U2OS cells showed a less pronounced reduction in signal intensity compared to their HepG2 cell counterpart, with the signal remaining visible in the cytoplasmic region surrounding the nuclei (Figure 5b).

Subsequently, we replicated these analyses with RPE-1 cells, a cell line derived from the retinal pigment epithelium. These immortalized nontumor cells maintain a stable genome and are emerging as an alternative to cancer cells.[46] The results are listed in Figure 5. Both FITC- and Nile Red-encapsulated micelles **1** produced an extremely reduced signal compared to that of HepG2 and U2OS cells, as quantified in Figure 5c. Specifically, FITC fluorescence was barely detectable, while Nile Red produced a faint signal with a distribution pattern similar to that observed for U2OS (Figure 5b).

In summary, our results demonstrate that the polymeric micelles used in this study exhibit a higher internalization rate for HepG2 cells compared to other cell types. However, the recognition capacity is not exclusive to hepatic cells, as some internalization is still observable in other cell types. Importantly, when micelles lacking the directing ligand lactonolactone were employed, no signal was observed either in U2OS or in RPE-1 (data not shown), consistent with our previous observations in HepG2 cells. Therefore, the observed phenomenon of micelle internalization observable in other cell types, although reduced, relies on the recognition of the directing ligand by receptors on the cell surface.

Our data demonstrate a greater internalization capacity for these micelles in osteosarcoma cancer cells compared with the nontumor cells analyzed. One plausible explanation could be associated with the well-described phenomenon of glucose transporter (GLUT) overexpression on the membrane of cancer cells due to the Warburg effect.[47−49] GLUTs may act as receptors recognizing the galactose terminal unit of lactonolactone, allowing for some internalization of micelles. Consequently, the addition of galactose terminal units to some cancer-targeting complexes has been employed as a strategy to enhance internalization in osteosarcoma cells.[50]

Furthermore, micelle internalization is also observed in nontumor cells investigated (RPE-1 cells), albeit to a lesser extent. This is more evident for Nile Red-encapsulated micelles compared with FITC-encapsulated micelles (Figure 5c). The Nile Red fluorophore produced a higher signal than FITC in both cell types. Despite the slightly increased EE of the micelles for Nile Red (Table 1), other factors might contribute to these differences. One such factor may be related to the free or hydrophobic/lipid-associated signaling dynamic of FITC and Nile Red fluorophores, respectively. Under reduced loading conditions, this may influence the occurrence of external diffusion or entrapment at specific cellular territories for these fluorophores.

Taken together, our results demonstrate a higher internalization rate of polymeric micelles in hepatic HepG2 cells compared to the nonhepatic cells analyzed. Moreover, nonhepatic cellular uptake is also influenced by the interaction of the directing ligand with external receptors, likely GLUT-related. Finally, this phenomenon was more pronounced in osteosarcoma cancer cells probably due to the overexpression of GLUT receptors in the cell membrane, one of the mechanisms fulfilling the glucose addiction of tumors.[49]

4. CONCLUSIONS

In this study, four different polymeric micelles have been prepared (**1**−**4**), based on chitosan as a polymeric core and lactonolactone residues as a potential hepatic-specific target ligand. The primary objective was to explore the internalization and disaggregation properties in both hepatic and nonhepatic cellular models. Moreover, the behavior of these micelles was evaluated through the encapsulation of two different fluorescent probes, namely, FITC or Nile Red. To comprehensively understand their internalization and disaggregation dynamics under physiological conditions, along with assessing potential cytotoxicity, confocal live-cell imaging was employed as an analytical methodology. Our findings clearly indicate that the presence of lactonolactone residues is required for the internalization of these micelles within cells. Moreover, we demonstrated that the disaggregation capacity of these nanocarriers is contingent upon the cystamine redox-sensitive linker embedded in the polymer. This linker reacts with intracellular GSH, elucidating the mechanism underlying the disaggregation process. Importantly, no cytotoxic effects were observed throughout the duration of our experiments. Lastly, we unveiled a heightened selectivity of these nanocarriers toward HepG2 cells in comparison to other nonhepatic cell models. In that sense, polymeric micelle **1**, as presented herein, emerges as a promising vehicle for drug delivery into hepatocytes and for application in the treatment of PHs. Nevertheless, further studies are still required to optimize and enhance the selection of these nanocarriers, specifically for hepatocytes.

■ ASSOCIATED CONTENT

Supporting Information

The Supporting Information is available free of charge at https://pubs.acs.org/doi/10.1021/acsomega.4c03415.

S1 video, HepG2 cells recorded after washout from treatment with FITC-encapsulated micelles 1 for 3 h; S2 video, HepG2 cells recorded after washout from treatment with NileRed-encapsulated micelles 1 for 3 h; and S3 video, HepG2 cells recorded after washout from treatment with a micelle-free solvent for 3 h (ZIP)

■ AUTHOR INFORMATION

Corresponding Author

Alfonso Alejo-Armijo − *Departamento de Química Inorgánica y Orgánica, Facultad de Ciencias Experimentales, Universidad de Jaén, 23071 Jaén, Spain;* Present Address: Departamento de Ciencias Farmacéuticas, Facultad de Farmacia, Universidad de Salamanca; Campus Miguel de Unamuno, 37007 Jaén, Spain; orcid.org/0000-0001-8691-4628; Email: aalejo@usal.es

Authors

María Ángeles Fernández-Mimbrera − *Departamento de Biología Experimental, Facultad de Ciencias Experimentales, Universidad de Jaén, 23071 Jaén, Spain*

Sofía Salido − *Departamento de Química Inorgánica y Orgánica, Facultad de Ciencias Experimentales, Universidad*

https://doi.org/10.1021/acsomega.4c03415
ACS Omega 2024, 9, 39503−39512

de Jaén, 23071 Jaén, Spain; orcid.org/0000-0003-2319-7873

Juan Alberto Marchal − *Departamento de Biología Experimental, Facultad de Ciencias Experimentales, Universidad de Jaén, 23071 Jaén, Spain*

Complete contact information is available at: https://pubs.acs.org/10.1021/acsomega.4c03415

Author Contributions

S.S., J.A.M., and A.A.-A. designed the experiments. M.A.F.-M., J.A.M., and A.A.-A. performed the experiments. All authors analyzed the results. A.A-A. and J.A.M. wrote the main manuscript text, and all authors reviewed the manuscript. All authors have given approval to the final version of the manuscript.

Funding

This work was supported by the Andalusian *Consejería de Economía y Conocimiento* (FEDER program 2014−2020: project numbers 1380682 and 1380808) and by PID2022−141783OB-C22/AEI/10.13039/501100011033/FEDER, UE.

Notes

The authors declare no competing financial interest.

■ ACKNOWLEDGMENTS

The authors express their gratitude to Nieves de la Casa (CICT, Universidad de Jaén, Spain) for technical assistance. Technical and human support provided by CICT of Universidad de Jaén (UJA, MINECO, Junta de Andalucía, FEDER) is gratefully acknowledged.

■ REFERENCES

(1) Grocholski, C.; Dubourg, L. D.; Guebre-Egziabher, F.; et al. Oxalate: from physiology to pathology. *Nephrol. Ther.* **2023**, *19*, 201−214.
(2) Fargue, S.; Acquaviva-Bourdain, C. Primary hyperoxaluria type 1: pathophysiology and genetics. *Clin. Kidney J.* **2022**, *15*, i4−i8.
(3) Rosenstock, J. L.; Joab, T. M. J.; DeVita, M. V.; et al. Oxalate nephropathy: a review. *Clin. Kidney J.* **2022**, *15*, 194−204.
(4) Salido, E.; Pey, A. L.; Rodríguez, R.; et al. Primary hyperoxalurias: Disorders of glyoxylate detoxification. *Biochim. Biophys. Acta* **2012**, *1822*, 1453−1464.
(5) Moya-Garzón, M. D.; Gomez-Vidal, J. A.; Alejo-Armijo, A.; et al. Small-molecule-based enzyme inhibitors in the treatment of primary hyperoxalurias. *Pers. Med.* **2021**, *11*, 74−103.
(6) Baltazar, P.; Ferreira de Melo, A.; Moreira, N.; et al. Oxalate (dys)metabolism: Person-to-person variability, kidney and cardiometabolic toxicity. *Genes* **2023**, *14*, 1719.
(7) Hoppe, B.; Martín-Higueras, C. Improving treatment options for primary hyperoxaluria. *Drugs* **2022**, *82*, 1077−1094.
(8) Garrelfs, S. F.; Frishberg, Y.; Hulton, S. A.; et al. Lumasiran, an RNAi therapeutic for primary hyperoxaluria type 1. *N. Engl. J. Med.* **2021**, *384*, 1216−1226.
(9) Kang, C. Lumarisan: A review in primary hyperoxaluria type 1. *Drugs* **2024**, *84*, 219−226.
(10) Hoppe, B.; Koch, A.; Cochat, P.; et al. Safety, pharmacodynamics, and exposure-response modeling results from a first-inhuman phase 1 study of nedosiran (PHYOX1) in primary hyperoxaluria. *Kidney Int.* **2022**, *101*, 626−634.
(11) Lai, C.; Pursell, N.; Gierut, J.; et al. Specific inhibition of hepatic lactate dehydrogenase reduces oxalate production in mouse models of primary hyperoxaluria. *Mol. Ther.* **2018**, *26*, 1983−1995.
(12) Syed, Y. Y. Nedosiran: First Approval. *Drugs* **2023**, *83*, 1729−1733.
(13) Moya-Garzón, M. D.; Martín-Higueras, C.; Peñalver, P.; et al. Salicylic acid derivatives inhibit oxalate production in mouse hepatocytes with primary hyperoxaluria type 1. *J. Med. Chem.* **2018**, *61*, 7144−7167.
(14) Lowther, W. T.; Holmes, R. P. Glycolate oxidase inhibitors and methods of use for the treatment of kidney stones. U.S. Patent WO2017100266 (A1), 2017.
(15) Alejo-Armijo, A.; Cuadrado, C.; Salido, S.; et al. Lactate dehydrogenase A (LDHA) inhibitors with a 2,8 dioxabicyclo[3.3.1]-nonane scaffold: a contribution to molecular therapies for primary hyperoxalurias. *Bioorg. Chem.* **2022**, *129*, No. 106127.
(16) Salido, S.; Alejo-Armijo, A.; Altarejos, J. Synthesis and hLDH inhibitory activity of analogues to natural products with 2,8-dioxabicyclo[3.3.1]nonane scaffold. *Int. J. Mol. Sci.* **2023**, *24*, 9925.
(17) Díaz, I.; Salido, S.; Nogueras, M.; et al. Design and synthesis of new pyrimidine-quinolone hybrids as novel hLDHA inhibitors. *Pharmaceuticals* **2022**, *15*, 792−821.
(18) Moya-Garzón, M. D.; Rodriguez-Rodriguez, B.; Martin-Higueras, C.; et al. New salicylic acid derivatives, double inhibitors of glycolate oxidase and lactate dehydrogenase, as effective agents decreasing oxalate production. *Eur. J. Med. Chem.* **2022**, *237*, No. 114396.
(19) Ding, J.; Gumpena, R.; Boily, M.-O.; et al. Dual glycolate oxidase/lactate dehydrogenase A inhibitors for primary hyperoxaluria. *ACS Med. Chem. Lett.* **2021**, *12*, 1116−1123.
(20) Granchi, C.; Bertini, S.; Macchia, M.; et al. Inhibitors of lactate dehydrogenase isoforms and their therapeutic potentials. *Curr. Med. Chem.* **2010**, *17*, 672−697.
(21) Fiume, L.; Manerba, M.; Vettraino, M.; et al. Inhibition of lactate dehydrogenase activity as an approach to cancer therapy. *Future Med. Chem.* **2014**, *6*, 429−445.
(22) Yuan, N.; Shao, K.; Huang, S.; et al. Chitosan, alginate, hyaluronic acid and other novel multifunctional hydrogel dressing for wound healing: A review. *Int. J. Biolog. Macromol.* **2023**, *240*, No. 124321.
(23) An, Z.; Dong, Y.; Wang, W.; et al. Preparation of pH-sensitive carboxymethyl chitosan nanoparticles loaded with ginsenoside Rb1 and evaluation of drug release in vitro. *Int. J. Biolog. Macromol.* **2024**, *267*, No. 131487.
(24) Zhang, W.; Zhang, Q.; Yang, Y.; et al. Multi-functional chitosan polymeric micelles for improving the oral bioavailability of paclitaxel based on synergistic effect. *Drug Delivery Transl. Res.* **2024**.
(25) Ali, A.; Ahmed, S. A review on chitosan and its nanocomposites in drug delivery. *Int. J. Biol. Macromol.* **2018**, *109*, 273−286.
(26) Majumder, N.; Das, N. G.; Das, S. K. Polymeric micelles for anticancer drug delivery. *Ther. Delivery* **2020**, *11*, 613−635.
(27) Salido, S.; Alejo-Armijo, A.; Parola, A. J.; et al. Chitosan derivatives as nanocarrierrs for hLDHA inhibitors delivery to hepatic cells: A selective strategy for targeting primary hyperoxaluria diseases. *Int. J. Pharm.* **2022**, *627*, No. 122224.
(28) Anderson, M. E. Glutathione: an overview of biosynthesis and modulation. *Chem. Biol. Interact.* **1998**, *111*, 1−14.
(29) Roggenbuck, D.; Mytilinaiou, M. G.; Lapin, S. V.; et al. Asialoglycoprotein receptor (ASGPR): a peculiar target of liver-specific autoimmunity. *Autoimmun. Highlights* **2012**, *3*, 119−125.
(30) Greenspan, P.; Mayer, E. P.; Fowler, S. D. Nile Red a selective fluorescent stain for intracellular lipid droplets. *J. Cell Biol.* **1985**, *100*, 965−973.
(31) Fowler, S. D.; Greenspan, P. Application of Nile Red, a fluorescent hydrophobic probe for the detection of neutral lipid deposits in tissue sections. *J. Histochem. Cytochem.* **1985**, *33*, 833−836.
(32) Wu, D.-Q.; Lu, B.; Chang, C.; et al. Galactosylated fluorescent labeled micelles as a liver targeting drug carrier. *Biomaterials* **2009**, *30*, 1363−1371.
(33) Trubitsyn, G.; Nguyen, V. N.; Di Tommaso, C.; et al. Impact of covalently Nile Red and covalently Rhodamine labeled fluorescent polymeric micelles for the improved imaging of the respective drug delivery system. *Eur. J. Pharm. Biopharm.* **2019**, *142*, 480−487.

(34) Herrero-Ruíz, A.; Martínez-García, P. M.; Terrón-Bautista, J.; et al. Topoisomerase IIα represses transcription by enforcing promoter-proximal pausing. *Cell Reports* **2021**, *35*, No. 108977.
(35) Arroyo, M.; Trimborn, M.; Sánchez, A.; et al. Chromosome structure deficiencies in MCPH1 syndrome. *Chromosome* **2015**, *124*, 491−501.
(36) Schindelin, J.; Arganda-Carreras, I.; Frise, E.; et al. Fiji: an open-source platform for biological-image analysis. *Nat. Methods* **2012**, *9*, 676−682.
(37) Shi, Z.; Guo, R.; Li, W.; et al. Nanoparticles of deoxycholic acid, polyethylene glycol and folic acid-modified chitosan for targeted delivery of doxorubicin. *J. Mater. Sci: Mater. Med.* **2014**, *25*, 723−731.
(38) Zalipsky, S.; Harris, J. M. Introduction to chemistry and biological applications of poly (ethylene glycol). In *Poly(ethylene glycol): chemistry and biological applications*; Harris, J. M.; Zalipsky, S. Eds.; American Chemical Society Library: Washington DC, 1997; Chapter 1, pp 1−13.
(39) Sackett, D. L.; Wolff, J. Nile red as a polarity-sensitive fluorescent probe of hydrophobic protein surfaces. *Anal. Biochem.* **1987**, *167*, 228−234.
(40) Garg, S.; De, A.; Nandi, T.; et al. Synthesis of a smart gold nano-vehicle for liver specific drug delivery. *AAPS Pharm. Sci. Technol.* **2013**, *14*, 1219−1226.
(41) Huo, M.; Liu, Y.; Wang, L.; et al. Redox-sensitive micelles based on O, N-hydroxyethyl chitosanoctylamine conjugates for triggered intracellular delivery of paclitaxel. *Mol. Pharmaceutics* **2016**, *13*, 1750−1762.
(42) Zaremba-Czogalla, M.; Jaromin, A.; Sidoryk, K.; et al. Evaluation of the in vitro cytotoxic activity of caffeic acid derivatives and liposomal formulation against pancreatic cancer cell lines. *Materials* **2020**, *13*, 5813.
(43) Cadete, A.; Olivera, A.; Besev, M.; et al. Self-assembled hyaluronan nanocapsules for the intracellular delivery of anticancer drugs. *Sci. Rep.* **2019**, *9*, 11565.
(44) Arzumanian, V. A.; Kiseleva, O. I.; Poverennaya, E. V. The curious case of the HepG2 cell line: 40 years of expertise. *Int. J. Mol. Sci.* **2021**, *22*, 13135.
(45) Cerrato, G.; Humeau, J.; Sauvat, A.; et al. Assessment of transcription inhibition as a characteristic of immunogenic cell death. *Methods Cell Biol.* **2022**, *172*, 67−82.
(46) Scott, S. J.; Suvarna, K. S.; D'Avino, P. P. Synchronization of human retinal pigment epithelial-1 cells in mitosis. *J. Cell Sci.* **2020**, *133*, jcs247940.
(47) Liu, C.; Jin, Y.; Fan, Z. The mechanism of Warburg effect induced chemoresistance in cancer. *Front. Oncol.* **2021**, *11*, No. 698023.
(48) Zambrano, A.; Molt, M.; Uribe, E.; et al. Glut 1 in cancer cells and the inhibitory action of resveratrol as a potential therapeutic strategy. *Int. J. Mol. Sci.* **2019**, *20*, 3374.
(49) Ancey, P.-B.; Contat, C.; Meylan, E. Glucose transporters in cancer − from tumor cells to the tumor microenvironment. *FEBS Journal* **2018**, *285*, 2926−2943.
(50) Moynihan, E.; Panseri, S.; Bassi, G.; et al. Development of novel Pt(IV)-carbohydrate derivatives as targeted anticancer agents against osteosarcoma. *Int. J. Mol. Sci.* **2023**, *24*, 6028.

https://doi.org/10.1021/acsomega.4c03415
ACS Omega 2024, 9, 39503−39512